Current Alzheimer Research, 2016, *13*, 1040-1047

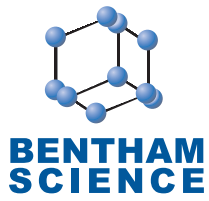

Decreased Myelinated Fibers in the Hippocampal Dentate Gyrus of the Tg2576 Mouse Model of Alzheimer's Disease

Wei Lu[1,3,#], Shu Yang[2,#], Lei Zhang[1], Lin Chen[1], Feng-Lei Chao[1], Yan-min Luo[1], Qian Xiao[1], Heng-Wei Gu[1], Rong Jiang[1] and Yong Tang[1,*]

[1]*Department of Histology and Embryology, Chongqing Medical University, Chongqing 400016, P.R. China;* [2]*Department of Histology and Embryology, Capital Medical University, Beijing 100069, P.R. China;* [3]*Department of Pediatrics, Navy General Hospital, Beijing 100069, P.R. China*

Yong Tang

Abstract: Alzheimer's disease (AD), the most common cause of dementia in the elderly, is characterized by deficits in cognition and memory. Although amyloid-β (Aβ) accumulation is known to be the earliest pathological event that triggers subsequent neurodegeneration, how Aβ accumulation causes behavioral deficits remains incompletely understood. In this study, using the Morris water maze test, ELISA and stereological methods, we examined spatial learning and memory performance, the soluble Aβ concentration and the myelination of fibers in the hippocampus of 4-, 6-, 8- and 10-month-old Tg2576 AD model mice. Our results showed that spatial learning and memory performance was significantly impaired in the Tg2576 mice compared to the wild type (WT) controls and that the myelinated fiber length in the hippocampal dentate gyrus (DG) was markedly decreased from 0.33 ± 0.03 km in the WT controls to 0.17 ± 0.02 km in the Tg2576 mice at 10 months of age. However, the concentrations of soluble $A\beta_{40}$ and $A\beta_{42}$ were significantly increased as early as 4-6 months of age. The decreased myelinated fiber length in the DG may contribute to the spatial learning and memory deficits of Tg2576 mice. Therefore, we suggest that the significant accumulation of soluble Aβ may serve as a preclinical biomarker for AD diagnosis and that protecting myelinated fibers may represent a novel strategy for delaying the progression of early-stage AD.

Keywords: Alzheimer's disease, Aβ, hippocampus, myelinated fiber, stereology, Tg2576 mouse.

Received: June 03, 2015 **Revised: November 26, 2015** **Accepted: December 08, 2015**

INTRODUCTION

Alzheimer's disease (AD), the most common cause of dementia in the elderly, is a progressive neurodegenerative disorder characterized by cognitive and memory defects. A greater understanding of the preclinical brain changes that occur in AD might facilitate earlier diagnosis and treatment of this disease. Several hypotheses have been proposed regarding the pathogenesis of AD. For example, senile plaques composed of progressively accumulated amyloid-β (Aβ) and neurofibrillary tangles composed of the hyperphosphorylated protein Tau are typical findings in the brains of AD patients; these observations support the most common hypothesis concerning AD, the Aβ cascade hypothesis [1-3]. This hypothesis proposes that Aβ accumulation initiates a complex cascade including neuronal dysfunction and loss and synaptic insufficiency that ultimately impairs memory and cognitive functions [4]. However, several studies using AD animal models have found inconsistencies between certain behavioral deficits and Aβ plaque deposition, challenging this hypothesis [5-7]. Another common hypothesis regarding AD is that neuronal loss is responsible for AD pathogenesis; however, this hypothesis has also been challenged by quantitative studies in both AD patients and mice [8-10]. These studies reported that there was no or only mild neuronal death in the cortex despite clear behavioral abnormalities. This discrepancy between the pathology and the behavioral manifestations of AD implies that additional pathological mechanisms underlie AD, especially during the early stages in which synapses are destroyed prior to Aβ plaque formation and neuronal loss [6]. One currently available method to address this issue is to use an AD animal model that recapitulates critical time-dependent aspects of AD. Tg2576 transgenic mice generated by Hsiao *et al.* express Aβ protein precursor (AβPP) and show memory and pathophysiological deficits similar to those of AD patients [5]. Notably, Tg2576 mice do not develop Aβ plaques until an advanced age (~18 months) and do not show neuronal death [5, 9]. Therefore, we selected the Tg2576 mouse model to investigate the potential myelinated fiber changes in AD progression.

In the present study, we estimated spatial learning ability, the hippocampal Aβ concentration and hippocampal fiber length and volume in Tg2576 mice. We demonstrated that the Aβ concentration was dramatically increased as early as 4-6 months of age but that spatial learning was not impaired until 10 months of age, when the myelinated fiber length in

*Address correspondence to this author at the Department of Histology and Embryology, Chongqing Medical University, Chongqing 400016, P.R. China; Tel & Fax: 86-23-6848-5589; E-mail: ytang062@163.com

[#]*Wei Lu and Shu Yang contributed equally to this work.*

1875-5828/16 $58.00+.00

the hippocampal dentate gyrus (DG) was markedly decreased.

MATERIALS AND METHODS

AD Mouse Model

Male Tg2576 (APP695SWE) and non-transgenic wild type (WT) control mice at 4, 6, 8 and 10 months of age were purchased from the Model Animal Research Center of Nanjing University (Nanjing, China); 15 mice were used in each group. Tg2576 mice express the human 695-amino acid isoform of AβPP carrying the double Swedish mutation (Lys670→Asn and Met671→Leu), resulting in the accumulation of both $A\beta_{40}$ and $A\beta_{42}$ peptides. All mice were maintained under a constant 12-h light/dark cycle at 22 ± 2℃ and were allowed access to water and standard chow diet *ad libitum*. All experiments were performed in accordance with the Guidelines for Animal Experimentation of Chongqing Medical University. The experimental procedures were approved by the Institutional Review Board of Chongqing Medical University, P. R. China.

Morris Water Maze (MWM)

The MWM task, which included a platform test and a probe test, was used to evaluate spatial learning and memory function. A MWM pool with a diameter of 1.2 m was divided into 4 quadrants and filled with water (22-25℃) that was rendered opaque using powdered milk. An escape platform with a diameter of 12 cm was placed in 1 quadrant (target quadrant) and submerged 1 cm beneath the surface of the water. The platform test was conducted for 6 consecutive days and for 4 trials per day. The mice were placed on the platform for 15 s before being placed in the water. The starting position was changed in each trial, and the sequence of the 4 starting positions varied daily. The mice were given a maximum of 90 s to reach the platform in each trial. Mice that failed to reach the platform within 90 s were guided to the platform and were allowed to remain on the platform for 15 s. The swim time and the swim path were monitored and measured using a SLY-WMS Morris System (Sunny Instruments, Beijing). On the 7^{th} day, the platform was removed from the pool, and the mice were subjected to 2 probe trials. The percentage of time spent in the target quadrant and the target zone was recorded. All experimental procedures were performed while blinded to the experimental groups.

ELISA

Following the MWM experiment, 6 mice from each group were randomly selected and intraperitoneally anesthetized via an overdose of 1% pentobarbital sodium following sedation with ether. The hippocampus was isolated, homogenized in guanidine buffer (5 M guanidine HCl and 50 mM Tris-HCl, pH 8.0), and diluted in Dulbecco's phosphate-buffered saline containing 5% BSA and 0.03% Tween-20 (DPBS-BSAT) supplemented with a protease inhibitor cocktail (Roche). The homogenate was centrifuged at 16,000×g at 4℃ for 20 min. The total protein concentration was determined using a BCA Protein Assay kit (Thermo), and the soluble $A\beta_{40}$ and $A\beta_{42}$ concentrations in the hippocampus were detected using Aβ ELISA kits (KHB3481 and KHB3441, respectively, Invitrogen), according to the manufacturer's instructions. Briefly, a 96-well ELISA plate was loaded with standards or samples mixed with the specific primary antibody in duplicate. The plate was incubated for 3 hrs at 25℃. After washing, the HRP-conjugated secondary antibody was applied for 30 min at 25℃, followed by treatment with the chromogen for 30 min. The reaction was terminated via the addition of a stop solution, and the optical density (OD) at 450 nm was measured using a microplate reader (BioRad550). The concentrations of soluble $A\beta_{40}$ and $A\beta_{42}$ were calculated according to the standard curve and were adjusted based on the total protein concentration.

Stereological Analysis

Tissue Processing

From the remaining 9 mice in 10-month old mice, 5 were randomly selected for the following stereological analysis. After sedation with ether, the mice were intraperitoneally anesthetized using 1% pentobarbital sodium (35 mg/kg) and perfusion-fixed with 2% paraformaldehyde and 2.5% glutaraldehyde in 0.1 M phosphate buffered saline (PBS, pH 7.4). The cerebral hemispheres were separated and coronally sliced into 1-mm-thick successive slabs.

Estimation of the Hippocampal Volume

A 50-μm section was sliced from each slab from the caudal surface using a cryostat (Leica CM3050S). After staining with hematoxylin, the entire hippocampus, the CA1 and the DG were outlined and photographed using a microscope (Olympus bx51) (Supplementary Fig. **S1**). The areas of the entire hippocampus, the CA1 and the DG were measured using a Visiopharm Integrator System (VIS, Visiopharm, Denmark), and the volumes of the entire hippocampus (V_{hip}), the CA1 (V_{CA1}) and the DG (V_{DG}) were calculated as the products of the area of the entire hippocampus, the CA1 or the DG and the slab thickness according to Cavalieri's principle [11, 12].

Sampling and Ultrathin Section Preparation

The cerebral slabs were sampled in a systematic, random manner. An equidistant-points probe was randomly overlapped on the image of the section from the sampled slabs using the VIS (Supplementary Fig. **S1**). The tissue blocks (1 mm^3) were sampled at the points on the hippocampus. On average, 5-6 tissue blocks from the entire hippocampus of each hemisphere were sampled, including 2-3 blocks in the CA1 and 2-3 blocks in the DG.

Isotropic, uniform and random (IUR) ultrathin sections were prepared using the "isector" technique as previously described [11, 12]. The 60-nm ultrathin sections were viewed under a transmission electron microscope (TEM, Hitachi-7500, Japan). At a magnification of 8,000X, 15 fields of view from each ultrathin section were imaged in a simple random manner (Fig. **1**).

Estimation of the Myelinated Fiber Length in the Hippocampus

An unbiased counting frame was randomly overlaid onto each TEM photograph. The myelinated fiber profiles within the counting frame or touching the inclusion lines were

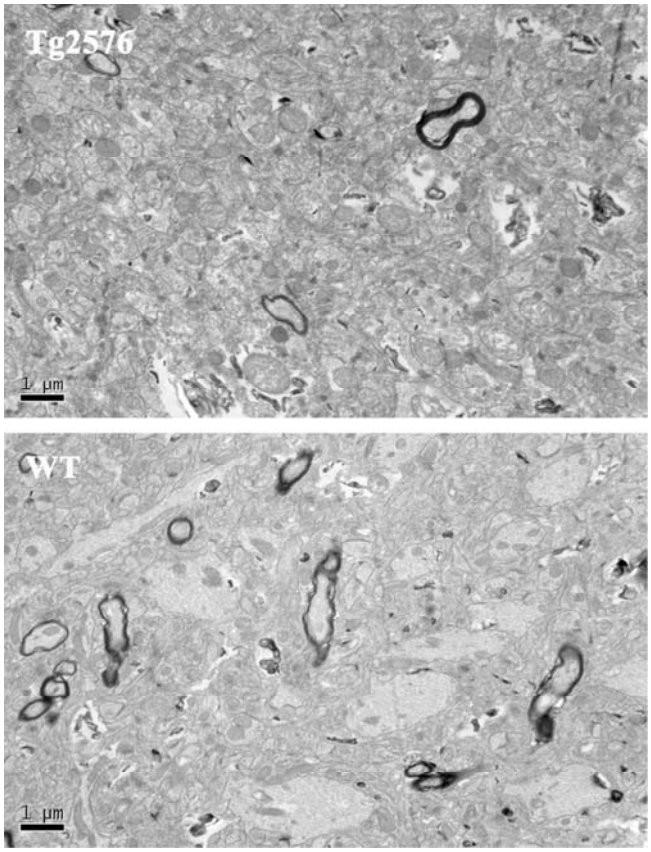

Fig. (1). Representative TEM images of the hippocampus of Tg2576 and WT control mice.

counted, and those touching the exclusion lines were excluded from the count [11, 12] (Supplementary Fig. **S2**). The length density of the myelinated fibers in the entire hippocampus ($Lv_{mf/hip}$), the CA1 ($Lv_{mf/CA1}$) and the DG ($Lv_{mf/DG}$) were estimated according to Yang *et al.* [11, 12] as follows:

$$Lv_{mf/hip} = 2 \times \sum Q_{mf,\ hip} / [a(frame) \times \sum frames]$$
$$Lv_{mf/CA1} = 2 \times \sum Q_{mf,\ CA1} / [a(frame) \times \sum frames]$$
$$Lv_{mf/DG} = 2 \times \sum Q_{mf,\ DG} / [a(frame) \times \sum frames]$$

where $\sum Q_{mf,\ hip}$, $\sum Q_{mf,\ CA1}$ and $\sum Q_{mf,\ DG}$ denote the total number of myelinated fiber profiles counted in the entire hippocampus, CA1 and DG per brain, respectively; a(frame) denotes the area associated with a frame; and $\sum$frames denotes the total number of frames used.

$Lv_{mf/hip}$, $Lv_{mf/CA1}$ and $Lv_{mf/DG}$ were multiplied by V_{hip}, V_{CA1} and V_{DG}, respectively, to obtain the total length of the myelinated fibers in the entire hippocampus ($L_{mf,\ hip}$), the CA1 ($L_{mf,\ CA1}$) and the DG ($L_{mf,\ DG}$), respectively, as follows [11, 12].

$$L_{mf,\ hip} = Lv_{mf/hip} \times V_{hip}$$
$$L_{mf,\ CA1} = Lv_{mf/CA1} \times V_{CA1}$$
$$L_{mf,\ DG} = Lv_{mf/DG} \times V_{DG}$$

yvehol final samples representeGG, V(DG)reach the platform.

Estimation of the Myelinated Fiber Volume and the Myelin Sheath Volume in the Hippocampus

A counting grid with equidistant points was randomly superimposed onto each TEM photograph. The points on the myelinated fibers in the entire hippocampus ($\sum P_{mf,\ hip}$), the CA1 ($\sum P_{mf,\ CA1}$) or the DG ($\sum P_{mf,\ DG}$), on the myelin sheaths in the entire hippocampus ($\sum P_{ms,\ hip}$), the CA1 ($\sum P_{ms,\ CA1}$) or the DG ($\sum P_{ms,\ DG}$) and on the entire hippocampus ($\sum P_{hip}$), the CA1 ($\sum P_{CA1}$) or the DG ($\sum P_{DG}$) were counted. The volume density of the myelinated fibers in the entire hippocampus ($Vv_{mf/hip}$), the CA1 ($Vv_{mf/CA1}$) and the DG ($Vv_{mf/DG}$) and the volume density of the myelin sheath in the entire hippocampus ($Vv_{ms/hip}$), the CA1 ($Vv_{ms/CA1}$) and the DG ($Vv_{ms/DG}$) were estimated according to Yang *et al.* [11, 12] (Fig. **S2**).

$$Vv_{mf/hip} = \sum P_{mf,\ hip} / \sum P_{hip}$$
$$Vv_{mf/CA1} = \sum P_{mf,\ CA1} / \sum P_{CA1}$$
$$Vv_{mf/DG} = \sum P_{mf,\ DG} / \sum P_{DG}$$
$$Vv_{ms/hip} = \sum P_{ms,\ hip} / \sum P_{hip}$$
$$Vv_{ms/CA1} = \sum P_{ms,\ CA1} / \sum P_{CA1}$$
$$Vv_{ms/DG} = \sum P_{ms,\ DG} / \sum P_{DG}$$

Each volume density was multiplied by the total volume of the corresponding region to obtain the total volume of the myelinated fibers in the entire hippocampus ($V_{mf,\ hip}$), the CA1 ($V_{mf,\ CA1}$) or the DG ($V_{mf,\ DG}$) and the total volume of the myelinated sheaths in the entire hippocampus (V_{ms}, hip), the CA1 (V_{ms}, CA1) or the DG (V_{ms}, DG) as follows [11, 12].

$$V_{mf,\ hip} = Vv_{mf/hip} \times V_{hip}$$
$$V_{mf,\ CA1} = Vv_{mf/CA1} \times V_{CA1}$$
$$V_{mf,\ DG} = Vv_{mf/DG} \times V_{DG}$$
$$V_{ms,\ hip} = Vv_{ms/hip} \times V_{hip}$$
$$V_{ms,\ CA1} = Vv_{ms/CA1} \times V_{CA1}$$
$$V_{ms,\ DG} = Vv_{ms/DG} \times V_{DG}$$

Tissue Shrinkage

To avoid shrinkage artifacts, we calculated tissue processing-induced shrinkage as described previously [12, 13]. One tissue block was randomly sampled from each hippocampus. The area of the coronal surface of each block, A (before), was estimated using point counting. The tissue blocks were then processed in the same manner as described above. The area of the coronal surface of each block, A (after), was estimated using point counting after processing. A (before) and A (after) were compared to detect any shrinkage.

Statistics

The results were expressed as the means ± SEM. Statistical analysis was performed using SPSS version 13.0. The MWM data were averaged within groups for each session and were analyzed using a one-way repeated-measures analysis of variance (ANOVA) for the platform trials and a

one-way ANOVA for the probe trial, in which Group was the independent variable. The ELISA data, which did not display a normal distribution, were analyzed using a non-parametric test. The stereological data were compared using a Student *t*-test. The coefficient of error (CE) and the observed inter-brain coefficient of variation (OCV) for each measurement were estimated as previously described [11, 12]. A p value of 0.05 was adopted as the threshold for significance.

RESULTS

It has previously been reported that body weight affects behavioral performance [14]. To avoid this potential interference, we measured the body weight and the cerebral weight, neither of which was significantly different between the age-matched Tg2576 and WT mice (data not shown).

MWM Task

Neither the swim time nor the swim distance on the platform trials was significantly different between the Tg2576 and WT mice in the 4-, 6- or 8-month-old groups (Table **1** and **2**). In contrast, the swim time and the swim distance on the platform trials for the 10-month-old Tg2576 mice were markedly increased compared with the age-matched WT controls ($p < 0.05$) (Table **1** and **2**). However, the percentage of time spent in the target quadrant and the target zone on the probe trial was not significantly different between the Tg2576 and WT mice in any age group (Fig. **2**).

Soluble Aβ Concentration

The concentration of soluble $A\beta_{40}$ in the hippocampus was dramatically increased in the 4-, 6-, 8- and 10-month-old Tg2576 mice compared with the age-matched WT controls (Supplementary Table **S1**). The concentration of soluble $A\beta_{42}$ in the hippocampus was also increased in the 6-, 8- and 10-month-old Tg2576 mice compared with the age-matched WT controls, but no difference in the soluble $A\beta_{42}$ concentration was observed between the 4-month-old Tg2576 and WT mice (Supplementary Table **S1**).

Stereological Estimations

Because only the 10-month-old Tg2576 mice exhibited apparent behavioral deficits, we only analyzed the hippocampal changes in the 10-month-old mice. The hippocampal

Table 1. Swim time in platform trial.

Session (day)		1	2	3	4	5	6
4 months	WT (s)	54.2 ± 2.0	55.9 ± 1.3	51.9 ± 3.1	43.4 ± 3.7	38.1 ± 4.0	33.4 ± 5.1
	Tg2576 (s)	53.6 ± 2.0	55.5 ± 2.5	52.0 ± 2.8	52.1 ± 3.0	44.9 ± 4.4	42.2 ± 4.9
6 months	WT (s)	43.9 ± 3.8	37.5 ± 3.7	39.1 ± 4.5	35.6 ± 3.4	43.4 ± 3.4	35.5 ± 4.0
	Tg2576 (s)	49.2 ± 2.7	40.6 ± 2.6	38.0 ± 3.7	37.2 ± 3.0	37.6 ± 2.2	33.9 ± 2.6
8 months	WT (s)	48.7 ± 2.2	38.5 ± 2.5	33.3 ± 3.1	31.5 ± 2.7	31.2 ± 2.1	31.4 ± 2.5
	Tg2576 (s)	45.7 ± 3.0	39.1 ± 3.3	33.5 ± 4.5	30.2 ± 3.7	34.5 ± 3.9	26.0 ± 2.6
10 months	WT (s)	42.1 ± 3.3	34.5 ± 2.5	38.5 ± 3.2	31.6 ± 4.1	30.0 ± 4.3	26.0 ± 3.8
	Tg2576 (s)	53.7 ± 2.4*	47.1 ± 3.7*	39.2 ± 3.0	38.7 ± 4.6	34.5 ± 3.5	35.2 ± 3.9

* $p < 0.05$ vs WT controls at the same time point.

Table 2. Swim distance in platform trial.

Session (day)		1	2	3	4	5	6
4 months	WT (m)	8.7 ± 0.4	7.3 ± 0.3	6.9 ± 0.5	5.8 ± 0.6	4.8 ± 0.6	3.8 ± 0.6
	Tg2576 (m)	8.6 ± 0.5	8.3 ± 0.5	7.2 ± 0.6	7.4 ± 0.5	6.5 ± 0.7	5.6 ± 0.8
6 months	WT (m)	5.8 ± 0.5	4.5 ± 0.5	4.2 ± 0.5	4.0 ± 0.4	4.4 ± 0.3	3.9 ± 0.5
	Tg2576 (m)	6.1 ± 0.5	5.1 ± 0.4	4.4 ± 0.4	2.2 ±0.3	4.0 ± 0.3	3.8 ± 0.3
8 months	WT (m)	7.0 ± 0.4	6.0 ± 0.4	4.9 ± 0.5	5.3 ± 0.6	4.9 ± 0.5	4.6 ± 0.4
	Tg2576 (m)	7.2 ± 0.6	5.2 ± 0.6	4.1 ± 0.6	4.2 ± 0.5	5.1 ± 0.6	3.3 ± 0.5
10 months	WT (m)	7.9 ± 0.9	6.8 ± 0.7	7.2 ± 0.6	5.4 ± 0.9	5.1 ± 0.9	4.0 ± 0.7
	Tg2576 (m)	7.3 ± 0.7	9.9 ± 0.9*	7.5 ± 0.8	8.8 ± 1.1	6.5 ± 0.9	6.5 ± 0.9

* $p < 0.05$ vs WT controls at the same time point.

shrinkage caused by histological processing was not significantly different between the groups and did not bias the conclusions of the study (data not shown). The CEs were less than 10% (the recommended percentage), indicating that the variance introduced by the stereological sampling procedure was a minor portion of the observed variance (Table **3**).

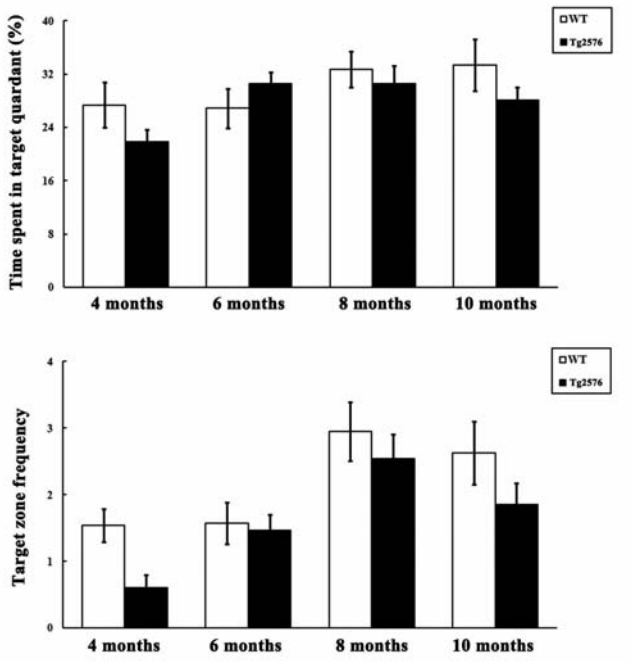

Fig. (2). The percentage of time spent in the target quadrant and the target zone during the probe trial on the 7th day was not significantly different between the Tg2576 and WT mice.

We failed to detect any significant volumetric changes in the entire hippocampus (26.8 ± 1.0 mm^3 vs. 24.7 ± 0.4 mm^3), the CA1 (9.3 ± 0.4 mm^3 vs. 8.8 ± 0.3 mm^3) or the DG (3.6 ± 0.3 mm^3 vs. 3.6 ± 0.1 mm^3) between the Tg2576 and WT mice (Fig. **3**). For the Tg2576 and WT mice, the total volume of the myelinated fibers was 0.56 ± 0.05 mm^3 and 0.78 ± 0.07 mm^3, respectively, in the entire hippocampus, 0.22 ± 0.02 mm^3 and 0.24 ± 0.02 mm^3, respectively, in the CA1, and 0.06 ± 0.01 mm^3 and 0.08 ± 0.01 mm^3, respectively, in the DG; the total volume of the myelin sheaths was 0.31 ± 0.02 mm^3 and 0. 38 ± 0.03 mm^3, respectively, in the whole hippocampus, 0.12 ± 0.01 mm^3 and 0.13 ± 0.01 mm^3, respectively, in the CA1, and 0.04 ± 0.00 mm^3 and 0.06 ± 0.01 mm^3, respectively, in the DG. No significant difference in the myelinated fiber or myelin sheath volume in any examined brain region was observed between the Tg2576 and WT mice (Fig. **3**). However, although the myelinated fiber length in the entire hippocampus and in the CA1 of Tg2576 mice was nearly the same as that in the WT controls (hippocampus: 1.36 ± 0.13 km vs. 1.91 ± 0.16 km; CA1: 0.50 ± 0.04 km vs. 0.53 ± 0.05 km), the myelinated fiber length in the DG was significantly decreased in the Tg2576 mice (0.17 ± 0.02 km) compared to the WT controls (0.33 ± 0.03 km) ($p < 0.05$, Fig. **3**).

DISCUSSION

Among the biomarkers for the diagnosis of AD, Aβ accumulation is the most determining factor [4]. Aβ peptides, which are proteolytically cleaved from AβPP and which are primarily composed of $A\beta_{40}$ and $A\beta_{42}$, can exist as soluble monomers, dimers, oligomers and insoluble polymers. Although high molecular weight Aβ polymers constitute the extracellular amyloid deposits in AD, soluble Aβ species are more cytotoxic because they are present both intra- and extra-cellularly and because they accumulate much earlier than the appearance of amyloid deposits [15-17]. Moreover, a wealth of evidence has indicated that the accumulation of soluble Aβ species, but not insoluble amyloid deposits, in the cortex and the hippocampus correlates with cognitive impairments in AD patients and animal models [18-20]. In the present study, we found that as early as 4 months, the soluble $A\beta_{40}$ concentration in the hippocampus of Tg2576 mice was significantly increased. Moreover, in accordance with Jacobsen *et al.* [6], we observed that the $A\beta_{42}$ concentration was significantly increased after 6 months. The apparent difference in the timing of $A\beta_{40}$ and $A\beta_{42}$ accumulation in Tg2576 mice might be due to the selective proteolytic processing of AβPP. Collectively, soluble Aβ species considerably accumulate in the hippocampus of Tg2576 mice from 4 to 6 months of age. However, spatial learning ability, as assessed by the MWM platform trials, was clearly reduced only in 10-month-old Tg2576 mice. The emergence of learning deficits in Tg2576 mice at 10 months of age has been observed previously [21]. These results suggested that soluble Aβ species might not be the direct cause of the behavioral deficits in AD. Furthermore, we did not detect any reference memory loss in Tg2576 mice based on the MWM probe trial, although this result may be due to the insensitivity of the probe trial in AD mice [22].

It is well-known that Aβ accumulation initiates the pathogenesis of AD, ultimately resulting in brain function deficits caused by multiple underlying pathological alterations, including microgliosis, astrocytosis, neuronal dysfunc-

Table 3. OCV and CE (n = 5).

		V_{hip}	V_{CA1}	V_{DG}	$L_{mf, hip}$	$L_{mf, CA1}$	$L_{mf, DG}$	$V_{mf, hip}$	$V_{mf, CA1}$	$V_{mf, DG}$	$V_{ms, hip}$	$V_{ms, CA1}$	$V_{ms, DG}$
WT	OCV(%)	3.2	8.3	7.5	19.3	21.6	20.1	21.8	21.7	21.4	20.4	17.8	18.6
	CE(%)	1.4	3.7	3.3	8.6	9.6	9.3	9.7	9.7	9.6	9.1	7.9	8.3
Tg2576	OCV(%)	8.0	9.1	17.6	22.1	20.4	19.8	18.4	18.9	18.3	17.1	17.9	22.1
	CE(%)	3.6	4.1	7.9	9.9	9.1	8.9	8.2	8.5	8.2	7.6	8.0	9.9

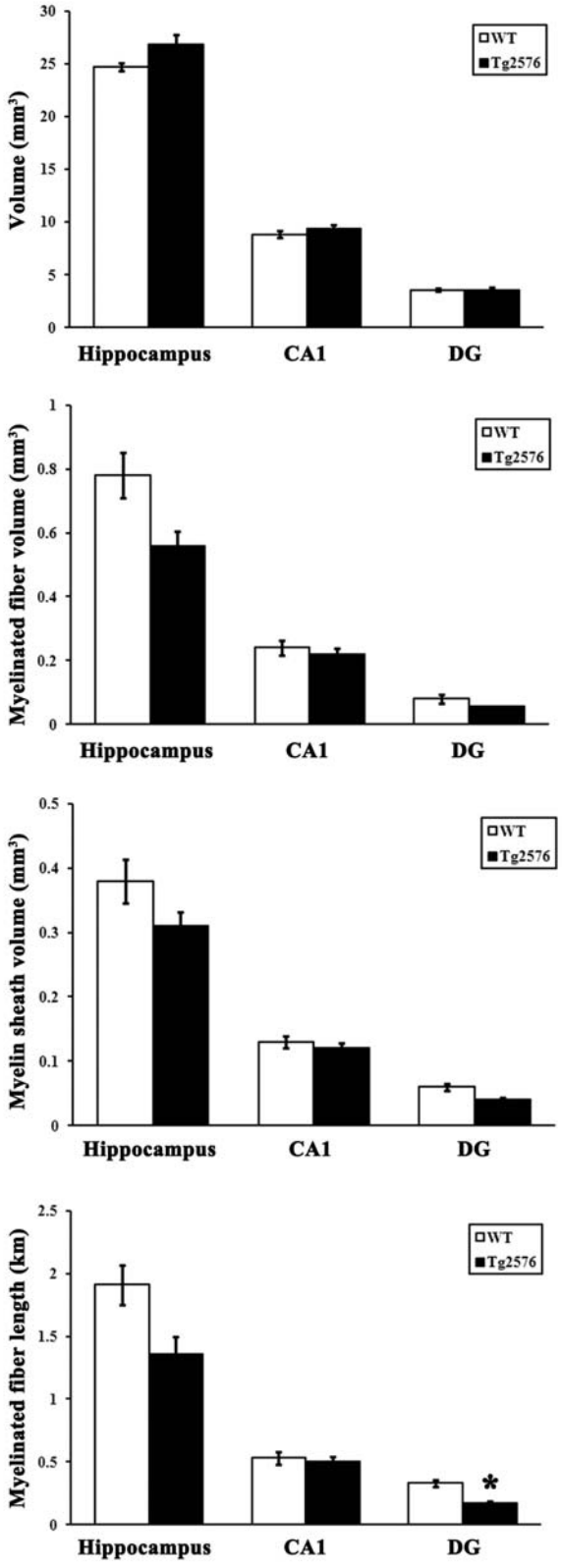

Fig. (3). No significant difference in the total volume, the myelinated fiber volume, or the myelinated sheath volume of the hippocampus, the CA1 or the DG was observed between the Tg2576 and WT mice at 10 months of age. However, the total length of the myelinated fibers in the DG was dramatically decreased in the 10-month-old Tg2576 mice compared to the WT control mice (* $p <$ 0.05).

tion and loss, synaptic insufficiency, neurotransmitter alterations [4] and other presently undetermined factors. The hippocampus is one of the most vulnerable brain regions in AD. Accumulating evidence from several studies suggests that hippocampal atrophy is strongly associated with the cognitive and memory deficits of AD patients and model mice [23-26]. Conversely, Barnes *et al.* [27] presented contrasting findings, in which hippocampal atrophy is not specific to AD. In the present study, we did not observe a significant decrease in the volume of the entire hippocampus, the CA1 or the DG of 10-month-old Tg2576 mice. This result indicates that hippocampal atrophy may not be an invariable biomarker for AD diagnosis, at least in the early stage. With respect to neurons in the hippocampus during AD progression, using stereological methods, Regeur *et al.* [8] demonstrated the lack of global neocortical neuronal loss in AD patients. Similarly, West *et al.* [28] did not observe significant neuronal loss in any subdivision of the hippocampus in preclinical AD patients. Furthermore, transgenic AD mice exhibit behavioral abnormalities prior to neuronal loss [29]. Regarding the synaptic changes in AD, Scheff *et al.* [30] found a significant decrease in the synaptic density of the outer molecular layer of the DG in AD patients. Further research has revealed that as early as 4 months of age, the spine density of the outer molecular layer of the DG is decreased in Tg2576 mice [6]. Thus, synaptic damage has been implicated in early AD [31].

Axon terminals are one of the most important components of synapses. Neuronal impulses are transferred via nerve fibers and are ultimately transmitted to downstream effectors via synapses. The breakdown of the nerve fibers may damage the integrity of neural circuits to impair cognition and memory. To test this hypothesis, we measured the volume and the length of the myelinated fibers in the hippocampus of Tg2576 mice. Our results showed that the total length of the myelinated fibers in the DG was significantly reduced in 10-month-old Tg2576 mice, and this result corresponded to the impairment in spatial learning performance. Jacobsen *et al.* [6] established the time-dependent neuronal alteration in the DG of Tg2576 mice; this alteration was categorized into early-onset (4-5 month-old) and late-onset stages (older than 12 months); the early-onset stage began with a decrease in spine density [6]. In this study, we further elucidated that synapses might be the most sensitive structure to soluble Aβ accumulation, followed by a decrease in myelinated fibers in the DG of Tg2576 mice. One limitation of this study was that we did not estimate the hippocampal myelinated fibers of 4-, 6- or 8-month-old Tg2576 mice; therefore, we could not define the earliest time point at which hippocampal myelinated fibers are decreased. Because the DG is a major site of synaptic input into the hippocampus, the neuroanatomical changes observed in this region imply that both synaptic and myelinated fiber changes are involved in the cognitive and memory deficits of early-stage AD model mice. The myelinated fiber decrease in early AD is unlikely to be caused by axonal deterioration because neuronal death does not occur until late AD. Alternatively, in early AD, when neurons are preserved, the myelinated fiber decrease might be attributed to potentially reversible demyelination.

Previous studies have also reported myelin abnormalities in AD. Carmeli *et al.* [32] assessed the myelin content in preclinical AD patients using the magnetization transfer ratio (MTR) and demonstrated demyelination in the hippocampus. In addition, Zerbi *et al.* [33] observed abnormal signaling of fiber tracts in the hippocampus of a mouse model of AD (APP(swe)/PS1(dE9)) that closely resembles the findings of axonal disconnection and myelin degradation in AD patients. Schmued *et al.* reported that conspicuous myelin pathology, such as edematous swelling of myelinated fibers, was frequently observed in the molecular and polymorph layers of the DG in transgenic AD model mice [34]. Combined with these previous findings, our results suggested that the myelinated fiber decrease which probably due to demyelination is a structural change during the early stages of AD and that protecting against demyelination represents a novel strategy for delaying early AD progression. Fortunately, a recent research by our group stated that running exercise could reverse the spatial learning damage by reducing the myelinated fiber loss in AD mice [35], further consolidating the myelinated fiber as a potential therapeutic target for AD treatment in early stage.

SUPPLEMENTARY MATERIAL

Supplementary material is available on the publisher's web site along with the published article.

CONFLICT OF INTEREST

The authors confirm that this article content has no conflict of interest.

ACKNOWLEDGEMENTS

This study was supported by the National Natural Science Foundation of China (NSFC 81470057, 31271288 and 81171238) and the Research Foundation for 100 Academic and Discipline Talented Leaders of Chongqing, P. R. China.

REFERENCES

[1] Hardy JA, Higgins GA. Alzheimer's disease: the amyloid cascade hypothesis. Science 256: 184-5 (1992).

[2] Hardy J, Selkoe DJ. The amyloid hypothesis of Alzheimer's disease: progress and problems on the road to therapeutics. Science 297: 353-6 (2002).

[3] Alafuzoff I, Arzberger T, Al-Sarraj S, Bodi I, Bogdanovic N, Braak H, *et al.* Staging of neurofibrillary pathology in Alzheimer's disease: a study of the BrainNet Europe Consortium. Brain Pathol 18: 484-96 (2008).

[4] Selkoe DJ. Toward a comprehensive theory for Alzheimer's disease. Hypothesis: Alzheimer's disease is caused by the cerebral accumulation and cytotoxicity of amyloid beta-protein. Ann N Y Acad Sci 924: 17-25 (2000).

[5] Hsiao K, Chapman P, Nilsen S, Eckman C, Harigaya Y, Younkin S, *et al.* Correlative memory deficits, Abeta elevation, and amyloid plaques in transgenic mice. Science 274: 99-102 (1996).

[6] Jacobsen JS, Wu CC, Redwine JM, Comery TA, Arias R, Bowlby M, *et al.* Early-onset behavioral and synaptic deficits in a mouse model of Alzheimer's disease. Proc Natl Acad Sci USA 103: 5161-6 (2006).

[7] Bories C, Guitton MJ, Julien C, Tremblay C, Vandal M, Msaid M, *et al.* Sex-dependent alterations in social behaviour and cortical synaptic activity coincide at different ages in a model of Alzheimer's disease. PLoS One 7: e46111 (2012).

[8] Regeur L, Jensen GB, Pakkenberg H, Evans SM, Pakkenberg B. No global neocortical nerve cell loss in brains from patients with senile dementia of Alzheimer's type. Neurobiol Aging 15: 347-52 (1994).

[9] Irizarry MC, McNamara M, Fedorchak K, Hsiao K, Hyman BT. APPSw transgenic mice develop age-related A beta deposits and neuropil abnormalities, but no neuronal loss in CA1. J Neuropathol Exp Neurol 56: 965-73 (1997).

[10] Irizarry MC, Soriano F, McNamara M, Page KJ, Schenk D, Games D, *et al.* Abeta deposition is associated with neuropil changes, but not with overt neuronal loss in the human amyloid precursor protein V717F (PDAPP) transgenic mouse. J Neurosci 17: 7053-9 (1997).

[11] Yang S, Li C, Zhang W, Wang WW, Nyengaard JR, Tang Y. Application of stereological method to study the white matter and myelinated fibers therein of rat brain. Image Anal Stereol 27: 125-32 (2008).

[12] Yang S, Li C, Zhang W, Wang WW, Tang Y. The myelinated fiber changes in the white matter of aged female Long-Evans rats. J Neurosci Res 87: 1582-90 (2009).

[13] Yang S, Li C, Qiu X, Zhang L, Lu W, Chen L, *et al.* Effects of an enriched environment on myelin sheaths in the white matter of rats during normal aging: A stereological study. Neuroscience 234: 13-21 (2013).

[14] Markowska AL. Sex dimorphisms in the rate of age-related decline in spatial memory: relevance to alterations in the estrous cycle. J Neurosci 19: 8122-33 (1999).

[15] LaFerla FM, Tinkle BT, Bieberich CJ, Haudenschild CC, Jay G. The Alzheimer's A beta peptide induces neurodegeneration and apoptotic cell death in transgenic mice. Nat Genet 9: 21-30 (1995).

[16] Walsh DM, Tseng BP, Rydel RE, Podlisny MB, Selkoe DJ. The oligomerization of amyloid beta-protein begins intracellularly in cells derived from humanbrain. Biochemistry 39: 10831-9 (2000).

[17] Zhang Y, McLaughlin R, Goodyer C, LeBlanc A. Selective cytotoxicity of intracellular amyloid beta peptide 1-42 through p53 and Bax in cultured primary human neurons. J Cell Biol 156: 519-29 (2002).

[18] Wang J, Dickson DW, Trojanowski JQ, Lee VM. The levels of soluble versus insoluble brain Abeta distinguish Alzheimer's disease from normal and pathologic aging. Exp Neurol 158: 328-37 (1999).

[19] Naslund J, Haroutunian V, Mohs R, Davis KL, Davies P, Greengard P, *et al.* Correlation between elevated levels of amyloid beta peptide in the brain and cognitive decline. JAMA 283: 1571-7 (2000).

[20] Zhang W, Hao J, Liu R, Zhang Z, Lei G, Su C, *et al.* Soluble Aβ levels correlate with cognitive deficits in the 12-month-old APPswe/PS1dE9 mouse model ofAlzheimer's disease. Behav Brain Res 222: 342-50 (2011).

[21] Kishimoto Y, Higashihara E, Fukuta A, Nagao A, Kirino Y. Early impairment in a water-finding test in a longitudinal study of the Tg2576 mouse model of Alzheimer's disease. Brain Res 1491: 117-26 (2013).

[22] Arendash GW, King DL, Gordon MN, Morgan D, Hatcher JM, Hope CE, *et al.* Progressive, age-related behavioral impairments in transgenic mice carrying both mutant amyloidprecursor protein and presenilin-1 transgenes. Brain Res 891: 42-53 (2001).

[23] Foster TC. Biological markers of age-related memory deficits: treatment of senescent physiology. CNS Drugs 20: 153-66 (2006).

[24] Wang PN, Liu HC, Lirng JF, Lin KN, Wu ZA. Accelerated hippocampal atrophy rates in stable and progressive amnestic mild cognitive impairment. Psychiatry Res 171: 221-31 (2009).

[25] Beauquis J, Vinuesa A, Pomilio C, Pavía P, Galván V, Saravia F. Neuronal and glial alterations, increased anxiety, and cognitive impairment before hippocampal amyloid deposition in PDAPP mice, model of Alzheimer's disease. Hippocampus 24: 257-69 (2014).

[26] Li X, Zheng L, Zhang J, Zhou X, Ma C, Chen Y, *et al.* Differences in functional brain activation and hippocampal volume among amnestic mild cognitive impairment subtypes. Curr Alzheimer Res 10: 1080-9 (2013).

[27] Barnes J, Whitwell JL, Frost C, Josephs KA, Rossor M, Fox NC. Measurements of the amygdala and hippocampus in pathologically confirmed Alzheimer disease and frontotemporal lobar degeneration. Arch Neurol 63: 1434-9 (2006).

[28] West MJ, Kawas CH, Stewart WF, Rudow GL, Troncoso JC. Hippocampal neurons in pre-clinical Alzheimer's disease. Neurobiol Aging 25: 1205-12 (2004).

[29] Calhoun ME, Wiederhold KH, Abramowski D, Phinney AL, Probst A, Sturchler-Pierrat C, *et al.* Neuron loss in APP transgenic mice. Nature 395: 755-6 (1998).

[30] Scheff SW, Sparks DL, Price DA. Quantitative assessment of synaptic density in the outer molecular layer of the hippocampal dentate gyrus in Alzheimer's disease. Dementia 7: 226-32 (1996).

[31] Masliah E, Crews L, Hansen L. Synaptic remodeling during aging and in Alzheimer's disease. J Alzheimers Dis 9: 91-9 (2006).

[32] Carmeli C, Donati A, Antille V, Viceic D, Ghika J, von Gunten A, *et al.* Demyelination in mild cognitive impairment suggests progression path to Alzheimer's disease. PLoS One 8: e72759 (2013).

[33] Zerbi V, Kleinnijenhuis M, Fang X, Jansen D, Veltien A, Van Asten J, *et al.* Gray and white matter degeneration revealed by diffusion in an Alzheimer mouse model. Neurobiol Aging 34: 1440-50 (2013).

[34] Schmued LC, Raymick J, Paule MG, Dumas M, Sarkar S. Characterization of myelin pathology in the hippocampal complex of a transgenic mouse model of Alzheimer's disease. Curr Alzheimer Res 10: 30-7 (2013).

[35] Chao F, Zhang L, Luo Y, Xiao Q, Lv F, He Q, *et al.* Running exercise reduces myelinated fiber loss in the dentate gyrus of the hippocampus in APP/PS1 transgenic mice. Curr Alzheimer Res 12: 377-83 (2015).